Brazilian Journal
of Chemical
Engineering

ISSN 0104-6632
Printed in Brazil
www.abeq.org.br/bjche

Vol. 32, No. 01, pp. 139 - 154, January - March, 2015
dx.doi.org/10.1590/0104-6632.20150321s00003129

INFLUENCE OF RESIDENCE-TIME DISTRIBUTION ON A SURFACE-RENEWAL MODEL OF CONSTANT-PRESSURE CROSS-FLOW MICROFILTRATION

W. Zhang[1] and S. G. Chatterjee[2*]

[1]Department of Civil and Environmental Engineering, 151 Link Hall
Syracuse University, Syracuse, New York 13244, USA.
[a]Presently at 3700 Windmeadows Blvd V228, Gainesville, Florida 32608, USA.
[2]Department of Paper and Bioprocess Engineering, SUNY College of Environmental
Science and Forestry, 1 Forestry Drive, Syracuse, New York 13210, USA.
Phone: +1-315-470-6517, Fax: +1-315-470-6945
E-mail: schatterjee@esf.edu

(Submitted: November 20, 2013 ; Revised: March 4, 2014 ; Accepted: March 17, 2014)

Abstract - This work examines the influence of the residence-time distribution (RTD) of surface elements on a model of cross-flow microfiltration that has been proposed recently (Hasan *et al*., 2013). Along with the RTD from the previous work (Case 1), two other RTD functions (Cases 2 and 3) are used to develop theoretical expressions for the permeate-flux decline and cake buildup in the filter as a function of process time. The three different RTDs correspond to three different startup conditions of the filtration process. The analytical expressions for the permeate flux, each of which contains three basic parameters (membrane resistance, specific cake resistance and rate of surface renewal), are fitted to experimental permeate flow rate data in the microfiltration of fermentation broths in laboratory- and pilot-scale units. All three expressions for the permeate flux fit the experimental data fairly well with average root-mean-square errors of 4.6% for Cases 1 and 2, and 4.2% for Case 3, respectively, which points towards the constructive nature of the model — a common feature of theoretical models used in science and engineering.
Keywords: Microfiltration; Residence-time distribution; Surface-renewal model.

INTRODUCTION

Cross-flow membrane filtration technology is widely used in the chemical and biotech industries globally, e.g., in the filtration of parenteral or biological liquids contaminated with charged particulates, for plasmapheresis, and in wastewater treatment. Depending upon the application, filtration membranes can be polymeric or ceramic. In cross-flow membrane filtration, an incoming feed solution or suspension flows across the surface of a membrane and the permeate flow is that portion of the liquid which passes through the membrane in a direction perpendicular to that of the main flow. The permeate flux is affected by the membrane material, liquid velocity, liquid viscosity, type of dissolved/suspended solids and their concentration, transmembrane pressure drop, temperature, and membrane fouling. As time progresses, permeate flow rate declines as the membrane fouls due to pore blocking, concentration polarization and cake-layer buildup.

A number of publications have used the surface-renewal concept to theoretically model cross-flow microfiltration and ultrafiltration (Koltuniewicz, 1992;

*To whom correspondence should be addressed

Koltuniewicz and Noworyta, 1994; Koltuniewicz and Noworyta, 1995; Constenla and Lozano, 1996; Arnot *et al*., 2000; Chatterjee, 2010; Sarkar *et al.*, 2011; Hasan *et al*., 2013). Compared to the film and boundary-layer models of membrane filtration, the surface-renewal model has the potential to more faithfully describe the transfer of dissolved/suspended solids due to random hydrodynamic impulses generated at the membrane surface, e.g., due to membrane roughness or by the use of spacers or turbulence promoters. Such instabilities, when introduced deliberately into the main flow (e.g., by means of Dean vortices), induce back migration of accumulated solute molecules or particulates away from the membrane surface and significantly enhance permeation rates (Mallubhotla and Belfort, 1997; Gehlert *et al*., 1998; Mallubhotla *et al*., 1998). Almeida *et al*. (2010) experimentally studied the effect of wall roughness and three different spacer configurations on the microflow hydrodynamics of deionized water flowing in slits for a Reynolds number range of 58−500. For five different relative roughness values of the bottom surface of the open channel, the measured longitudinal pressure drop departed from the Hagen−Poiseuille formula − increasing with increasing roughness and decreasing slit height. According to these authors, this indicated the presence of surface phenomena in such flows that are irrelevant in macroscale flows. In slits of 1.2 and 1.5 mm height, flow visualization in the longitudinal direction showed the presence of recirculation zones downstream of each spacer filament, whose extent increased as the Reynolds number increased. Above a critical Reynolds number in such slits, the flow became unstable, which was reflected in a change of slope of the Darcy friction factor versus Reynolds number plot. This transition was not observed in a 1-mm high slit, indicating the presence of transient structures in the flow for all values of the studied Reynolds number.

Recently, Hasan *et al*. (2013) presented a mathematical model of cross-flow microfiltration (CFMF) using the surface-renewal concept and classical cake-filtration theory for predicting permeate-flux decline and cake buildup on the membrane surface as a function of process time. The three model parameters R_m (membrane resistance), k_c [a parameter that is related to the specific cake resistance α − see Eq. (3)] and S (rate of renewal of liquid elements at the membrane surface) were estimated by fitting the model to experimental permeate flow rate data in the CFMF of fermentation broths in laboratory- and pilot-scale units. The parameter S, which is an increasing function of the velocity of the main flow as shown empirically by Koltuniewicz (1992), Koltuniewicz and Noworyta (1994) and Koltuniewicz and Noworyta (1995), can also be looked upon as a "scouring" term, which represents the removal of deposited material from the membrane wall (Arnot *et al.*, 2000) and which depends upon the level of flow instability. In contrast to the well-known critical-flux model of CFMF (intermediate-blocking and cake-filtration cases), the surface-renewal model of Hasan *et al*. (2013) provides explicit expressions for the permeate flux and cake mass as functions of process time, besides indicating the influence of transmembrane pressure drop, feed concentration and liquid velocity on the permeate flux. Hasan *et al*. (2013), however, did not empirically test the influence of these variables on the flux and left it for future work. As it currently stands, the surface-renewal model of Hasan *et al*. (2013) has no parameter that explicitly indicates the fouling regime (unlike the critical-flux model) since it assumes *a priori* that the primary cause of permeate flux decline is cake accumulation on the membrane surface with pore blocking occurring in the initial stages of filtration.

The present paper is a follow-up to the work of Hasan *et al*. (2013) and examines the influence of the residence-time distribution (RTD) of surface elements on their CFMF model. Along with the RTD from the previous work (Case 1), two other RTD functions (Cases 2 and 3) are used to develop theoretical expressions for the permeate-flux decline and cake buildup in the filter as a function of process time. The three different RTDs represent three different startup conditions of the filtration process. The analytical expressions for the permeate flux are tested by fitting them to the experimental permeate flow rate data that were reported in the earlier work (Hasan *et al*., 2013).

SURFACE-RENEWAL MODEL OF CROSS-FLOW MICROFILTRATION

In the surface-renewal model of cross-flow microfiltration (Hasan *et al*., 2013), it is postulated that the primary cause of permeate flux decline is cake accumulation on the membrane surface with the phenomenon of pore blocking occurring in the first moments of filtration, whose effects are included in the membrane resistance R_m (treated as an empirical parameter). Due to flow instabilities, fresh liquid elements continuously arrive at the membrane-liquid interface from the bulk liquid. A specific liquid element resides at the membrane surface for a definite time t, after which it returns to the bulk liquid, which is assumed to be well mixed, having a constant

suspended solids concentration of c_b. With the progress of time, a cake layer builds up on the surface, causing a gradual reduction of permeate flux with process time until it reaches a steady value. In order to model the microfiltration process, it is assumed that, during the residence time t of a liquid element at the membrane surface, permeate flux and cake accumulation within it can be modeled by classical cake-filtration theory (McCabe *et al*., 1993). The expression for the permeate or filtrate flux $J(t)$ in a surface element is given by (Hasan *et al*., 2013):

$$J(t) = \frac{1}{\sqrt{\left(1/J_0^2\right) + 2k_c t}} \tag{1}$$

where

$$J_0 = \frac{\Delta p}{\mu R_m} \tag{2}$$

and

$$k_c = \frac{\mu c_b \alpha}{\Delta p} \tag{3}$$

In the above, J_0 = permeate flux at time $t = 0$, Δp = transmembrane pressure drop, μ = viscosity of the filtrate, R_m = resistance of the membrane or filter medium, c_b = mass of solids deposited in the filter per unit volume of filtrate (approximately equal to the feed concentration), and α = specific cake resistance.

We now assume that the dominant flux of suspended solids to the membrane wall is that due to the convective motion of the liquid (driven by Δp) compared to the solid fluxes to and from the membrane surface due to the surface-renewal mechanism. The mass $m_c(t)$ of solids accumulated in the element per unit area of the membrane surface during the time period of t is then given by (Hasan *et al*., 2013):

$$m_c(t) = \int_0^t J(t) c_b dt = \frac{c_b}{k_c}\sqrt{\left(1/J_0^2\right) + 2k_c t} - \frac{c_b}{k_c J_0} \tag{4}$$

The surface of the membrane at any time t_p during the filtration process is visualized as being populated by a mosaic of liquid elements that have ages that range from zero to t_p. If we denote the age-distribution (i.e., RTD) function of the surface elements as $f(t, t_p)$, the age-averaged permeate flux (i.e., process flux) $J_a(t_p)$ and age-averaged cake mass accumulated per unit area of the membrane surface $m_{c,a}(t_p)$ at process time t_p can be expressed as (Hasan *et al*., 2013):

$$J_a(t_p) = \int_0^{t_p} J(t) f(t, t_p) dt \tag{5}$$

and

$$m_{c,a}(t_p) = \int_0^{t_p} m_c(t) f(t, t_p) dt \tag{6}$$

For later use, we define the following dimensionless quantities and also give the definition of the extended Euler gamma function $\Gamma(x, y)$:

$$S^* = \frac{S}{2k_c J_0^2} \tag{7}$$

$$t_p^* = S t_p \tag{8}$$

$$J_a^*\left(t_p^*\right) = \frac{J_a(t_p)}{J_0} \tag{9}$$

$$m_{c,a}^*\left(t_p^*\right) = \frac{m_{c,a}(t_p) J_0 k_c}{c_b} \tag{10}$$

$$\Gamma(x, y) = \int_y^\infty \lambda^{x-1} e^{-\lambda} d\lambda \tag{11}$$

where, as mentioned earlier, S (assumed to be constant) is the rate of renewal of liquid elements at the membrane surface.

Based on different speculative hypotheses about the behavior of liquid elements on the membrane wall, which correspond to different startup conditions, different RTD functions [i.e., $f(t, t_p)$] can be derived. These can then be used in Eqs. (5) and (6) to develop expressions for the permeate flux and cake buildup as shown next. Three cases with different RTD functions will be examined.

Case 1

This case was analyzed by (Hasan *et al*., 2013) and corresponds to a situation in which the membrane-liquid interface (assumed to be of unit area) is instantaneously and completely formed at $t_p = 0$ with liquid

elements flowing into it from the bulk liquid and departing from it to the bulk liquid at a constant rate for $t_p \geq 0$. If S is the surface-renewal rate, the fraction of the interface that is composed of elements with residence times between t and $t + dt$ at process time t_p is $f(t, t_p)dt$, with f being the RTD function, which is given by (Koltuniewicz and Noworyta, 1994; Hasan *et al*., 2013):

$$f\left(t,t_p\right)=\frac{Se^{-St}}{1-e^{-St_p}} \quad \text{for} \quad 0\leq t\leq t_p \tag{12}$$

As $t_p \to \infty$, it reduces to the steady-state, famous age-distribution function, i.e., Se^{-St}, which was originally proposed by Danckwerts (1951). Thus, Eq. (12) is an unsteady-state form of the Danckwerts age-distribution function. The cumulative fraction of surface elements that have ages lying in $0 \leq t \leq t_p$ can be obtained by integrating Eq. (12) with respect to t, i.e., the cumulative age-distribution function $F\left(t,t_p\right)$ is given by:

$$F\left(t,t_p\right)=\frac{1-e^{-St}}{1-e^{-St_p}} \quad \text{for} \quad 0\leq t\leq t_p \tag{12A}$$

Substituting Eqs. (1), (4) and (12) into Eqs. (5) and (6) and integrating yields (Hasan *et al*., 2013):

$$J_a^*\left(t_p^*\right)=\frac{e^{S^*}}{1-e^{-t_p^*}}\sqrt{\pi S^*} \left[\operatorname{erf}\left(\sqrt{S^*+t_p^*}\right)-\operatorname{erf}\left(\sqrt{S^*}\right)\right] \tag{13}$$

and

$$m_{c,a}^*\left(t_p^*\right)=\frac{e^{S^*}}{\left(1-e^{-t_p^*}\right)\sqrt{S^*}} \left[\Gamma\left(3/2,S^*\right)-\Gamma\left(3/2,S^*+t_p^*\right)\right]-1 \tag{14}$$

Case 2

The RTD function for this case is another unsteady-state form of the Danckwerts age-distribution function [see Eq. (18)], and has been previously presented by Chung *et al.* (1971) and Sada *et. al*. (1979). An elegant derivation of this RTD function, based on a stochastic population balance of interfacial fluid elements, has been provided by Fan *et al.* (1993). A derivation of the RTD function, which is based on physical arguments, is presented below for the benefit of the reader.

It is assumed that there are liquid elements, thought of as "blue," that are already present on the membrane surface (of unit area) at $t_p = 0$ when the filtration process starts and "red" elements start displacing the blue elements by the mechanism of surface renewal. At any time t_p, the surface will consist of a mixture of red and blue elements, the population of the latter decreasing as t_p increases. Permeate flow and cake accumulation are assumed to occur in all elements (red and blue) that constitute the membrane-liquid interface from $t_p = 0$ onwards. The red elements will have ages lying within $0 \leq t < t_p$ while the blue elements will all have ages of exactly t_p. At time t_p, the fraction of surface elements that are blue will be $e^{(-St_p)}$, while the other fraction will consist of red elements. Thus, we should have

$$\lim_{z\to t_p-}\int_0^z f\left(t,t_p\right)dt+e^{-St_p}=1 \tag{15}$$

We now assume that the RTD function of the red elements is given by:

$$f\left(t,t_p\right)=Ae^{-St},\ 0\leq t<t_p \tag{16}$$

where A is a constant. Substituting Eq. (16) into Eq. (15) yields:

$$\lim_{z\to t_p-}\int_0^z Ae^{-St}dt+e^{-St_p}=1 \tag{17}$$

Solving Eq. (17) gives $A = S$. Therefore, the overall RTD function is given by:

$$f\left(t,t_p\right)=Se^{-St}\left[1-u\left(t-t_p\right)\right]+\delta\left(t-t_p\right)e^{-St} \quad \text{for} \quad 0\leq t\leq t_p \tag{18}$$

where $u(t)$ and $\delta(t)$ are the unit step and delta functions, respectively. The cumulative age-distribution function corresponding to Eq. (18) is given by:

$$F\left(t,t_p\right)=\begin{cases}1-e^{-St} & \text{for} \quad 0\leq t<t_p\\ 1 & \text{at} \quad t=t_p\end{cases} \tag{19}$$

Equation (19) has a discontinuity at $t = t_p$ that becomes vanishingly small as $t_p \to \infty$. This discon-

tinuity is due to the fraction of surface elements at process time t_p that are blue, which, as mentioned earlier, is equal to e^{-St_p}. The age-averaged permeate flux $J_a(t_p)$ can be obtained by substituting Eq. (18) into Eq. (5), which yields:

$$J_a\left(t_p\right)=\int_0^{t_p} J\left(t\right)Se^{-St}dt+J\left(t_p\right)e^{-St_p} \tag{20}$$

The first and the second terms on the right-hand-side of Eq. (20) represent the contributions of the red and blue elements, respectively, to the flux. Substituting Eq. (1) into Eq. (20), integrating and using the dimensionless quantities defined earlier, yields the following expression for the permeate flux:

$$J_a^*\left(t_p^*\right)=e^{S^*}\sqrt{\pi S^*}\left[\operatorname{erf}\left(\sqrt{S^*+t_p^*}\right)-\operatorname{erf}\left(\sqrt{S^*}\right)\right]+\sqrt{\frac{S^*}{S^*+t_p^*}}\,e^{-t_p^*} \tag{21}$$

Using the RTD given by Eq. (18) in Eq. (6) gives:

$$m_{c,a}\left(t_p\right)=\int_0^{t_p} m_c\left(t\right)Se^{-St}dt+m_c\left(t_p\right)e^{-St_p} \tag{22}$$

Utilizing Eqs. (4) and (22) yields the following expression for the cake mass:

$$m_{c,a}^*\left(t_p^*\right)=\frac{e^{S^*}}{\sqrt{S^*}}\left[\Gamma\left(3/2,S^*\right)-\Gamma\left(3/2,S^*+t_p^*\right)\right]-1+\sqrt{\frac{S^*+t_p^*}{S^*}}\,e^{-t_p^*} \tag{23}$$

Case 3

The age-distribution function for this case is an extension of Case 2. The RTD function is summarized in Eq. (24):

$$f\left(t,t_p\right)=\begin{cases}\dfrac{1}{t_p} & \text{for } 0\le t\le t_p,\quad 0<t_p\le\dfrac{1}{S}\\ Se^{-St} & \text{for } 0\le t\le t_p-\dfrac{1}{S},\quad t_p>\dfrac{1}{S}\\ Se^{1-St_p} & \text{for } t_p-\dfrac{1}{S}<t\le t_p,\quad t_p>\dfrac{1}{S}\end{cases} \tag{24}$$

The membrane surface is assumed to be initially empty of liquid elements. At $t_p = 0$ when the filtration process starts, the surface starts filling up with such elements (with no outflow of elements) until a time $t_p = K/S$ when the surface-renewal mechanism is triggered and when liquid elements, which enter the interface from the bulk, start displacing those already occupying the membrane wall, which start flowing out of the interface to the bulk liquid. For simplicity (i.e., to avoid introducing an extra parameter), a value of $K = 1$ is assumed in the development that follows, which provides a derivation of the RTD function represented by Eq. (24).

During the time interval $0<t_p\le\frac{1}{S}$, the age-distribution function of the liquid elements at the membrane surface (which is filling up with such elements) will be uniform and equal to $1/t_p$, i.e.,

$$\int_0^{t_p} f\left(t,t_p\right)dt=\int_0^{t_p}\frac{1}{t_p}dt=1 \tag{25}$$

When surface renewal starts at $t_p = 1/S$, let all liquid elements already occupying the membrane wall at $t_p = 1/S$ be imagined to have the color "blue," while those liquid elements from the bulk that start displacing the blue elements from $t_p = 1/S$ onwards be thought of as being "red." A similar situation as that described in Case 2 prevails, i.e., at any time $t_p > 1/S$, the surface will consist of a mixture of red and blue elements with ages lying in the ranges of 0 to $t_p - 1/S$ and $t_p - 1/S$ to t_p, respectively. The RTD function for the red elements, all of which have ages in $0\le t\le t_p-\frac{1}{S}$, will be Se^{-St} while that for the blue elements, all of which have ages in $t_p-\frac{1}{S}<t\le t_p$, will be Se^{1-St_p} since

$$\int_0^{t_p} f\left(t,t_p\right)dt=\int_0^{t_p-1/S} Se^{-St}dt+\int_{t_p-1/S}^{t_p} Se^{1-St_p}dt=1 \tag{26}$$

Hence, equations for the permeate flux and cake mass can be derived depending upon the range in which the process time t_p lies. The cumulative age-distribution function corresponding to Eq. (24) is:

$$F(t,t_p)=\begin{cases}\dfrac{t}{t_p} & \text{for } 0\le t\le t_p,\quad 0<t_p\le\dfrac{1}{S}\\ 1-e^{-St} & \text{for } 0\le t\le t_p-\dfrac{1}{S},\ t_p>\dfrac{1}{S}\\ 1+Se^{1-St_p}(t-t_p) & \text{for } t_p-\dfrac{1}{S}<t\le t_p,\ t_p>\dfrac{1}{S}\end{cases} \quad (26A)$$

i) $0<t_p\le\frac{1}{S}$ (i.e., $0<t_p^*\le 1$)

Equation (5) becomes

$$J_a(t_p)=\int_0^{t_p}J(t)\frac{1}{t_p}dt \quad (27)$$

Upon substituting Eq. (1) into Eq. (27), the permeate-flux expression is found to be:

$$J_a^*\left(t_p^*\right)=\frac{2S^*}{t_p^*}\left(\sqrt{\frac{S^*+t_p^*}{S^*}}-1\right) \quad (28)$$

The cake mass $m_{c,a}(t_p)$ can be obtained from the following equation:

$$m_{c,a}\left(t_p\right)=\int_0^{t_p}m_c\left(t\right)\frac{1}{t_p}dt \quad (29)$$

Substituting Eq. (4) into Eq. (29) and integrating yields:

$$m_{c,a}^*\left(t_p^*\right)=\frac{2}{3}\frac{S^*}{t_p^*}\left[\left(\frac{S^*+t_p^*}{S^*}\right)^{\frac{3}{2}}-1\right]-1 \quad (30)$$

ii) $t_p>\frac{1}{S}$ (i.e., $t_p^*>1$)

Equation (5) becomes

$$J_a\left(t_p\right)=\int_0^{t_p-1/S}J\left(t\right)Se^{-St}dt+\int_{t_p-1/S}^{t_p}J\left(t\right)Se^{1-St_p}dt \quad (31)$$

Substituting Eq. (1) into Eq. (31) and integrating yields the following equation for the permeate flux:

$$J_a^*\left(t_p^*\right)=2S^*e^{1-t_p^*}\left(\sqrt{\frac{S^*+t_p^*}{S^*}}-\sqrt{\frac{S^*+t_p^*-1}{S^*}}\right)+e^{S^*}\sqrt{\pi S^*}\left[\operatorname{erf}\left(\sqrt{S^*+t_p^*-1}\right)-\operatorname{erf}\left(\sqrt{S^*}\right)\right] \quad (32)$$

The cake mass $m_{c,a}(t_p)$ is given by the following equation using the appropriate RTD [i.e., Eq. (24)]:

$$m_{c,a}\left(t_p\right)=\int_0^{t_p-1/S}m_c\left(t\right)Se^{-St}dt+\int_{t_p-1/S}^{t_p}m_c\left(t\right)Se^{1-St_p}dt \quad (33)$$

Substituting Eq. (4) into Eq. (33) and integrating yields:

$$m_{c,a}^*\left(t_p^*\right)=\frac{e^{S^*}}{\sqrt{S^*}}\left[\Gamma\left(3/2,S^*\right)-\Gamma\left(3/2,S^*+t_p^*-1\right)\right]-1+e^{1-t_p^*}\left\{\frac{2}{3}S^*\left[\left(\frac{S^*+t_p^*}{S^*}\right)^{\frac{3}{2}}-\left(\frac{S^*+t_p^*-1}{S^*}\right)^{\frac{3}{2}}\right]\right\} \quad (34)$$

We note that Eqs. (32) and (34) approach Eqs. (28) and (30), respectively, as $t_p^*\to 1$, i.e., the permeate flux and cake mass are continuous at $t_p^*=1$.

For all three cases (which use different RTD functions), it may be shown that as $t_p^*\to 0$

$$J_a^*\left(t_p^*\to 0\right)=1 \quad (35)$$

and

$$m_{c,a}^*\left(t_p^*\to 0\right)=0 \quad (36)$$

while as $t_p^*\to\infty$

$$J_a^*\left(t_p^*\to\infty\right)=\frac{J_a\left(t_p\to\infty\right)}{J_0}=\frac{J_{lim}}{J_0}=J_{lim}^*=e^{S^*}\sqrt{\pi S^*}\left[1-\operatorname{erf}\left(\sqrt{S^*}\right)\right] \quad (37)$$

and

$$m^*_{c,a}\left(t^*_p \to \infty\right) = m^*_{c,lim} = \frac{e^{S^*}}{\sqrt{S^*}}\Gamma\left(3/2, S^*\right) - 1 \qquad (38)$$

where J_{lim} is the value of the limiting or steady-state permeate flux and $m^*_{c,lim}$ is the steady-state value of the dimensionless cake mass.

Unlike laboratory or pilot-scale operation, industrial membrane filtration systems are generally not allowed to reach steady state. In order to maintain a high level of permeate flux, periodic backwashing is employed so as to regain the permeability of the membrane partially. Szwast *et al*. (2013) presented an integrated microfiltration model for concentrating a batch suspension in which each cycle consists of a normal period of operation in which the permeate flux declines with time followed by a period of backwashing in order to clean the membrane. Their model can predict the variation of the suspension concentration, permeate flux and temperature of the suspension with process time.

Table 1 presents a summary of the results for the three cases discussed earlier that correspond to the different RTD functions. It can be observed from this table that, in dimensionless coordinates, the permeate flux and cake mass are functions of process time with the surface-renewal rate being the only governing parameter.

The model parameters can be estimated as follows. From the experimental value of J_{lim} and Eq. (37), the dimensionless surface-renewal rate S^* can be determined, while the membrane resistance R_m can be calculated from the experimental value of the initial flux J_0 and Eq. (2). The surface-renewal rate S can then be estimated by fitting the permeate-flux expressions [i.e., Eqs. (13) or (21), or (28) and (32)] to experimental transient permeate-flux data so as to minimize the root-mean-square (RMS) deviation between predicted and experimental values of the flux. Finally, the values of k_c and α can be obtained from Eqs. (7) and (3), respectively.

Table 1: Expressions for the dimensionless permeate flux and dimensionless cake mass corresponding to the three different RTD functions.

Case	RTD $f(t, t_p)$	Dimensionless permeate flux $J^*_a(t^*_p)$	Dimensionless cake mass $m^*_{c,a}(t^*_p)$
1[a]	$\frac{Se^{-St}}{1-e^{-St_p}}$	$\frac{e^{S^*}}{1-e^{-t^*_p}}\sqrt{\pi S^*}\left[\mathrm{erf}\left(\sqrt{S^*+t^*_p}\right)-\mathrm{erf}\left(\sqrt{S^*}\right)\right]$	$\frac{e^{S^*}}{\left(1-e^{-t^*_p}\right)\sqrt{S^*}}\left[\Gamma\left(3/2,S^*\right)-\Gamma\left(3/2,S^*+t^*_p\right)\right]-1$
2	Se^{-St} for $0<t<t_p$ undefined at $t=t_p$	$e^{S^*}\sqrt{\pi S^*}\left[\mathrm{erf}\left(\sqrt{S^*+t^*_p}\right)-\mathrm{erf}\left(\sqrt{S^*}\right)\right]$ $+\sqrt{\frac{S^*}{S^*+t^*_p}}\,e^{-t^*_p}$	$\frac{e^{S^*}}{\sqrt{S^*}}\left[\Gamma\left(3/2,S^*\right)-\Gamma\left(3/2,S^*+t^*_p\right)\right]-1$ $+\sqrt{\frac{S^*+t^*_p}{S^*}}\,e^{-t^*_p}$
3	$\frac{1}{t_p}$ for $0\le t\le t_p, 0<t_p\le\frac{1}{S}$	$\frac{2S^*}{t^*_p}\left(\sqrt{\frac{S^*+t^*_p}{S^*}}-1\right)$	$\frac{2}{3}\frac{S^*}{t^*_p}\left[\left(\frac{S^*+t^*_p}{S^*}\right)^{\frac{3}{2}}-1\right]-1$
	Se^{-St} for $0\le t\le t_p-\frac{1}{S}, \quad t_p>\frac{1}{S}$	$2S^*e^{1-t^*_p}\left(\sqrt{\frac{S^*+t^*_p}{S^*}}-\sqrt{\frac{S^*+t^*_p-1}{S^*}}\right)$	$\frac{e^{S^*}}{\sqrt{S^*}}\left[\Gamma\left(3/2,S^*\right)-\Gamma\left(3/2,S^*+t^*_p-1\right)\right]-1$
	Se^{1-St_p} for $t_p-\frac{1}{S}<t\le t_p, \ t_p>\frac{1}{S}$	$+e^{S^*}\sqrt{\pi S^*}\left[\mathrm{erf}\left(\sqrt{S^*+t^*_p-1}\right)-\mathrm{erf}\left(\sqrt{S^*}\right)\right]$	$+e^{1-t^*_p}\left\{\frac{2}{3}S^*\left[\left(\frac{S^*+t^*_p}{S^*}\right)^{\frac{3}{2}}-\left(\frac{S^*+t^*_p-1}{S^*}\right)^{\frac{3}{2}}\right]\right\}$

[a] Hasan *et al*. (2013).

RESULTS AND DISCUSSION

In order to gain theoretical insight, Figures 1-4 show the influence of the surface-renewal rate on permeate-flux decline and cake buildup on the membrane surface as a function of process time in dimensionless coordinates for the three RTD cases discussed previously. In Figure 1 (S^* = 0.088), the permeate flux is the greatest for Case 1, lowest for Case 2 and intermediate for Case 3. For all three cases, the permeate flux declines with process time from an initial value of 1 to a limiting value of 0.39, which is a decrease of 61%. The inverse behavior is observed in Figure 2 in which Case 1 has the smallest growth of cake while Case 2 has the greatest, with Case 3 lying in between. For all three cases, the cake mass grows from an initial value of 0 to a steady-state value of 2.19. Increasing the surface-renewal rate S^* to 0.353 makes the corresponding curves for permeate flux and cake buildup for the three RTD cases come closer to one another (Figures 3 and 4) with the limiting permeate flux and cake mass reaching values of 0.60 and 0.85, respectively. Thus, increasing the surface renewal rate by a factor of 4 increases the limiting permeate flux by 54% while decreasing the limiting cakes mass by 61%, which shows the dramatic influence of the surface-renewal rate. From Eqs. (3) and (7) it can be deduced that an increased value of S^* implies a higher value of the ratio S/α. It is highly likely that in an actual cross-flow microfiltration run, α would decrease as S increases, which implies a looser, less compact cake, allowing a greater and easier flow of permeate besides the increased scouring effect due to the surface-renewal mechanism. It should be noted that Hasan *et al.* (2013) proposed a correlation for the surface-renewal rate S as a function of the liquid velocity in the main flow direction of the membrane channel, channel diameter and roughness, and viscosity and density of the feed suspension.

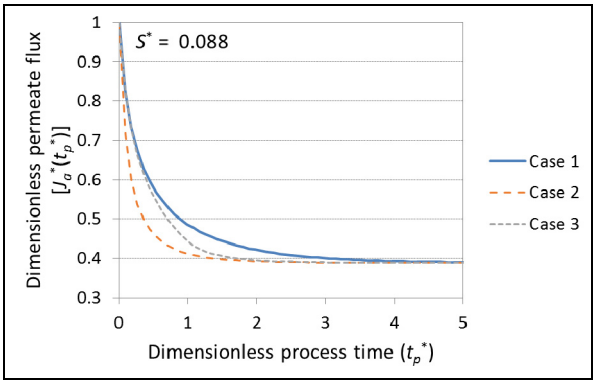

Figure 1: Behavior of the theoretical permeate flux as a function of process time in dimensionless coordinates (S^* = 0.088).

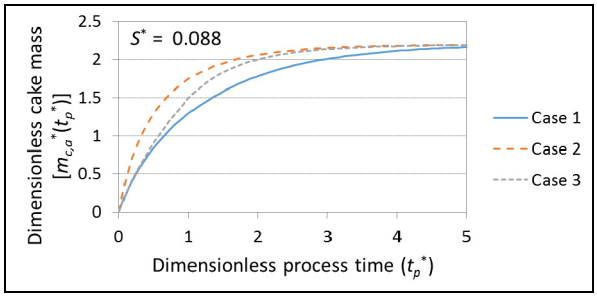

Figure 2: Behavior of the theoretical cake mass as a function of process time in dimensionless coordinates (S^* = 0.088).

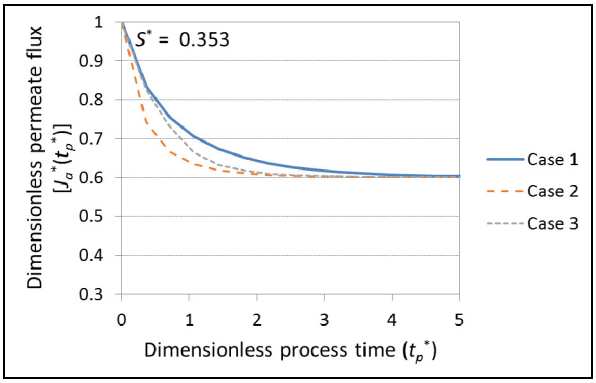

Figure 3: Behavior of the theoretical permeate flux as a function of process time in dimensionless coordinates (S^* = 0.353).

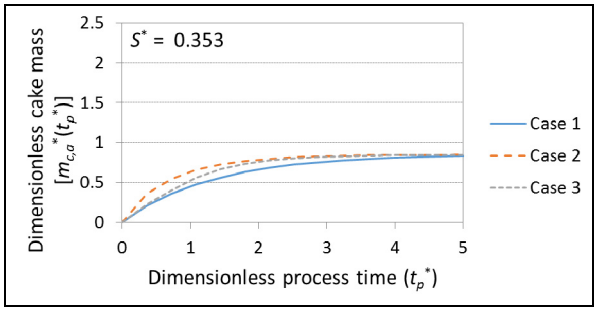

Figure 4: Behavior of the theoretical cake mass as a function of process time in dimensionless coordinates (S^* = 0.353).

To understand the behavior described in the previous paragraph, Table 2 summarizes expressions for the cumulative age-distribution function F, while Figures 5-7 show them as functions of the dimensionless residence time t^* (= St) and dimensionless process time t_p^*(= St_p) for the three RTD cases. For small values of t_p^*, the curves of F against t^* are quite different from one another. For example, at t_p^* = 0.9 and t^*= 0.6, the values of F are 0.76, 0.45 and 0.67 for Cases 1, 2 and 3, respectively. Thus, the population of younger elements at the membrane wall is greatest for Case 1 and smallest for Case 2, with that for Case 3 lying in between. Since younger elements have a higher permeate flux than older elements [see Eq. (1)], the age-averaged permeate flux is greatest for Case 1, followed by those for Cases 3 and 2, respectively (Figures 1 and 3), while cake buildup is smallest for Case 1, greatest for Case 2 and intermediate for Case 3, respectively (Figures 2 and 4). As t_p^* becomes large, the initial state of the membrane surface becomes more and more unimportant and F for the three cases approaches the cumulative steady-state age distribution function:

$$F\left(t^*, t_p^* \to \infty\right) = 1 - e^{-t^*} \tag{39}$$

In industrial cross-flow microfiltration of fermentation broths, the membrane module is often flushed initially with a buffer solution in order to equilibrate it (Ikuta, 2014). There will thus be liquid present on the membrane wall when filtration begins at t_p = 0. In such a situation, Case 2 would be more applicable than Cases 1 and 3. This, of course, does not account for the initial dilution effect of the feed solution due to the presence of the buffer solution in the module, nor does it account for the small time taken to reach the final transmembrane pressure drop, which is gradually raised in order to preserve membrane integrity. The three cases discussed in this paper are therefore highly idealized pictures of a very complex process.

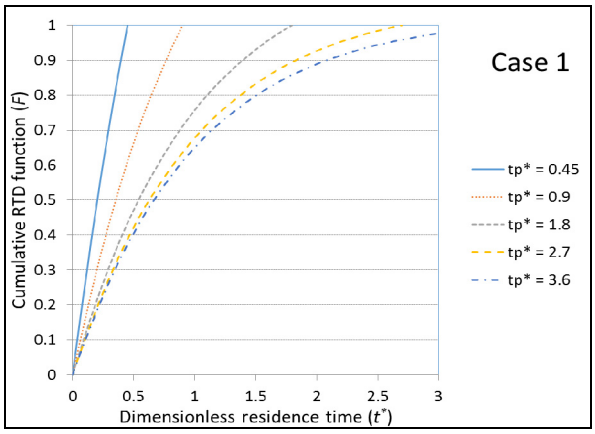

Figure 5: Cumulative residence-time distribution function for Case 1.

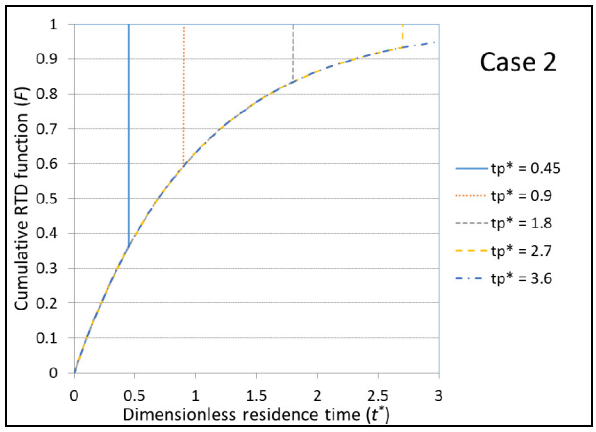

Figure 6: Cumulative residence-time distribution function for Case 2.

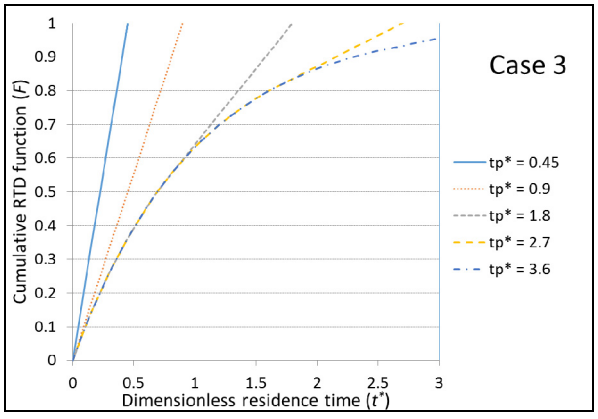

Figure 7: Cumulative residence-time distribution function for Case 3.

Table 2: Cumulative age-distribution functions corresponding to the three different RTD cases.

Case	RTD $F(t^*, t_p^*)$
1	$\frac{1-e^{-t^*}}{1-e^{-t_p^*}}$ for $0 \le t^* \le t_p^*$
2	$1-e^{-t^*}$ for $0 \le t^* < t_p^*$ 1 at $t^* = t_p^*$
3	$\frac{t^*}{t_p^*}$ for $0 \le t^* \le t_p^*,\ 0 < t_p^* \le 1$
	$1-e^{-t^*}$ for $0 \le t^* \le t_p^* - 1,\ t_p^* > 1$ $1+e^{1-t_p^*}(t^* - t_p^*)$ for $t_p^* - 1 < t^* \le t_p^*,\ t_p^* > 1$

We now turn to the work of Hasan *et al.* (2013), who performed cross-flow microfiltration experiments with fermentation broths in laboratory- and pilot-scale ceramic membrane units, which were conducted in total recycle mode, i.e., both permeate and retentate were continuously recirculated back to the feed vessel. They correlated their experimental permeate flow rate data with Eq. (13) of Case 1 and the reader is referred to their paper for a detailed discussion of the experimental conditions, experimental procedures and interpretation of the results. Their paper also compared predictions of the critical-flux model (Field *et al*., 1995) with their experimental permeate flow rate measurements.

In the current work, whose chief purpose is to examine the influence of the RTD of surface elements on permeate-flux decline and cake buildup, Eq. (21) [Case 2] and Eqs. (28) and (32) [Case 3] are fitted to the experimental data for the transient permeate flow rate of Hasan *et al*. (2013), a summary of whose experimental runs is provided in Table 3.

R_m of the clean membrane in the small-scale unit is estimated to be 1.14×10^{12} and 1.01×10^{12} m^{-1} for membrane pore sizes of 0.2 and 0.45 μm, respectively, while the main flow velocity in the same unit is estimated to be 1.3 m/s (Hasan *et al*., 2011). For the cross-flow microfiltration runs, the value of the viscosity μ of the filtrate necessary to calculate R_m from Eq. (2) was assumed to be the same as that of water at the experimental temperature (Perry *et al*., 1984; McCabe *et al*., 1993), i.e., the effects of substrate and salts on the viscosity were neglected.

As mentioned earlier, Hasan *et al*. (2013) have already presented the results for Case 1; for comparison purposes, these results are incorporated into the following discussion. Figures 8, 9 and 10 compare predictions of the three variants of the surface-renewal model with data for the permeate flow rate in the small-scale unit, while Figures 11 and 12 do the same for the pilot-scale unit. By fitting expressions for the permeate flux (Table 1) to these experimental data, optimum values of the three parameters (R_m, k_c and S) were estimated for each case − these are reported in Table 4 along with root-mean-square (RMS) deviations between the theoretical and experimental permeate flow rates.

Table 3: Summary of the cross-flow microfiltration experimental runs of Hasan *et al.* (2013).

Expt. no. and cell type	Fermentation medium and type	Initial optical density of broth @ 540 nm	Temp. °C	Δp kPa	Membrane unit type and area (m^2)	Membrane pore size (μm)	Membrane type
1. *Escherichia coli*	glucose, aerobic	53	21.8	206.84	small 0.13	0.45	ceramic
2. *Burkholderia cepacia*	glucose, aerobic	82	21.5	206.84	small 0.13	0.45	ceramic
3. *Pichia stipitis*	glucose, aerobic	72	22.8	206.84	small 0.13	0.45	ceramic
4. *Candida pseudotropicalis*	cheese whey, anaerobic	3	35.7	291.30	pilot 11.15	0.2	ceramic
5. *Candida pseudotropicalis*	glycerol, aerobic	66	46.9	207.60	pilot 11.15	0.2	ceramic

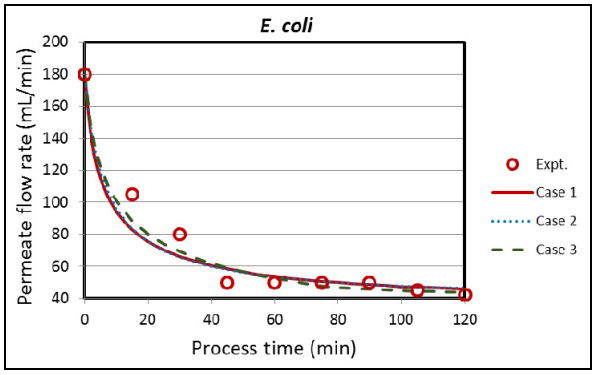

Figure 8: Comparison of theoretical and experimental (Hasan *et al*., 2013) permeate flow rates in the microfiltration of *E. coli* in the small-scale unit. Values of the model parameters are provided in Table 4 (expt. no. 1).

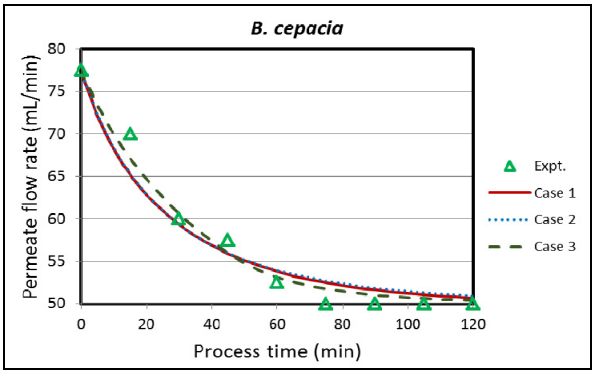

Figure 9: Comparison of theoretical and experimental (Hasan *et al*., 2013) permeate flow rates in the microfiltration of *B. cepacia* in the small-scale unit. Values of the model parameters are provided in Table 4 (expt. no. 2).

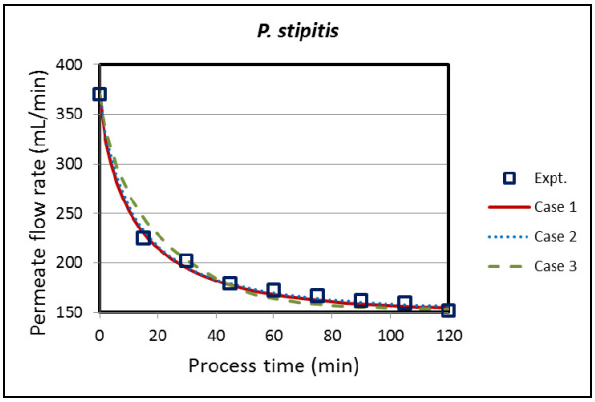

Figure 10: Comparison of theoretical and experimental (Hasan *et al*., 2013) permeate flow rates in the microfiltration of *P. stipitis* in the small-scale unit. Values of the model parameters are provided in Table 4 (expt. no. 3).

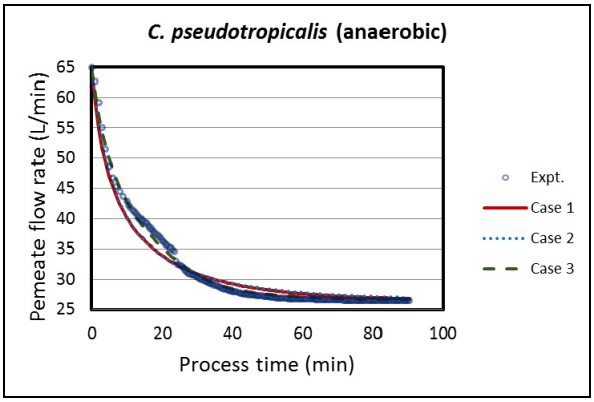

Figure 11: Comparison of theoretical and experimental (Hasan *et al*., 2013) permeate flow rates in the microfiltration of *C. pseudotropicalis* (grown under anaerobic conditions) in the pilot-scale unit. Values of the model parameters are provided in Table 4 (expt. no. 4).

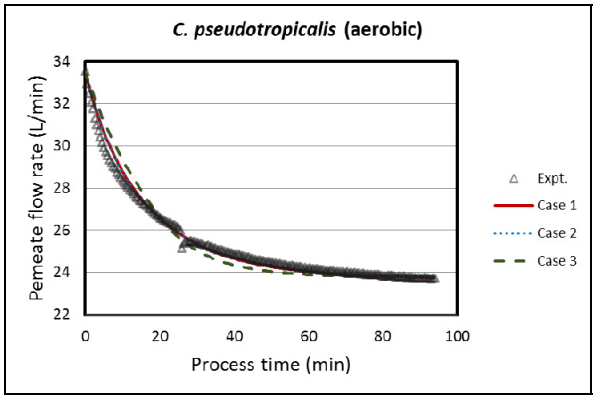

Figure 12: Comparison of theoretical and experimental (Hasan *et al*., 2013) permeate flow rates in the microfiltration of *C. pseudotropicalis* (grown under aerobic conditions) in the pilot-scale unit. Values of the model parameters are provided in Table 4 (expt. no. 5).

Table 4: Parameter values of the surface-renewal model for the three different RTD cases for the cross-flow microfiltration runs of Table 3.

Expt. no. and cell type	$R_m \times 10^{-13}$ m^{-1}	$k_c \times 10^{-6}$ s m^{-2}	$S \times 10^4$ s^{-1}	RMS error %
Case 1[a]				
1. *Escherichia coli*	0.812	11.323	3.0	12.0
2. *Burkholderia cepacia*	1.922	5.531	5.1	3.6
3. *Pichia stipitis*	0.368	1.063	5.0	2.5
4. *Candida pseudotropicalis (anaerobic)*	0.109	0.391	7.5	4.0
5. *Candida pseudotropicalis (aerobic)*	0.090	0.285	10.1	0.9
Average				4.6
Case 2				
1. *Escherichia coli*	0.812	4.152	1.1	12.0
2. *Burkholderia cepacia*	1.922	2.603	2.4	3.8
3. *Pichia stipitis*	0.368	0.425	2.0	2.3
4. *Candida pseudotropicalis (anaerobic)*	0.109	0.161	3.1	4.3
5. *Candida pseudotropicalis (aerobic)*	0.090	0.141	5.0	0.8
Average				4.6
Case 3				
1. *Escherichia coli*	0.812	8.681	2.3	10.5
2. *Burkholderia cepacia*	1.922	4.013	3.7	2.4
3. *Pichia stipitis*	0.368	0.744	3.5	4.7
4. *Candida pseudotropicalis (anaerobic)*	0.109	0.276	5.3	1.7
5. *Candida pseudotropicalis (aerobic)*	0.090	0.214	7.6	1.8
Average				4.2

[a] Hasan *et al*. (2013).

The work of Hasan *et al*. (2013) revealed that the nature of the cake resulting from different types of cells can lead to great differences in the values of R_m and k_c. The higher the values of these two parameters, the lower is the permeate flux, which can be observed in Figures 8−12. As can be seen from Table 4, in all three cases *P. stipitis* has the lowest value of k_c, followed by *B. cepacia* and *E. coli*, respectively. For the pilot-scale unit in which microfiltration of the same type of cells (*C. pseudotropicalis*) grown under anaerobic and aerobic conditions was performed, the values of k_c are of comparable magnitude for all the cases. R_m, which was calculated from the initial flux J_0 and Eq. (2) as mentioned earlier, ranges from 0.090–1.922×10^{13} m^{-1}, which is about 4 to19 times greater than the value of R_m of the clean membrane for the small-scale unit. It can also be observed from Table 4 that, for each experimental run, the estimated values of k_c and S are of the same order of magnitude for the three cases. Since the limiting-flux expression is the same for all the cases [i.e., Eq. (37)] from which the value of the dimensionless surface renewal rate S^* was calculated, the value of the ratio S/k_c should be the same for a particular run for all three cases [see Eq. (7)], although the individual magnitudes of S and k_c will be different. Thus, for Run 1 (*E. coli*), $S/k_c = 0.265 \times 10^{-10}$ m^2/s^2 for all the cases.

The experimental permeate flux declines with process time and eventually attains a steady-state value as predicted by theory, which can be seen in Figures 8−12 where it is also observed that, for all three cases, there is fairly good agreement between the theoretical and experimental permeate flow rates, which suggests that the three variants of the surface-renewal model examined in this work are more or less equivalent as regards the prediction of permeate-flux behavior (with predictions of Cases 1 and 2 being quite close to each other). This fact is corroborated in Table 4, where it is seen that the average RMS deviations between predicted and experimental values of the permeate flow rate are 4.6% for Case 1 and Case 2, and 4.2% for Case 3, respectively.

Figures 13−17 exhibit the predicted dimensionless, age-averaged cake mass $m_{c,a}^*$ as a function of the dimensionless process time t_p^* in the microfiltration of different types of cells in the small-scale and pilot-scale units. As the figures show, each curve starts at a value of zero and approaches a steady-state value as the filtration progresses. For a given value of t_p^*, the theoretical value of $m_{c,a}^*$ is highest for Case 2 followed by those for Cases 3 and 1, respectively. Since in the work of Hasan *et al*. (2013) only the optical density at 540 nm of the feed suspension was measured (Table 3) and not the actual cell concentration c_b, it was not possible to calculate values of the cake mass $m_{c,a}$ as a function of the process time t_p. For a particular experimental run (or cell type), the curves in Figs. 13−17 tend towards the same final steady-state value of the dimensionless cake mass given by Eq. (38) for all three cases.

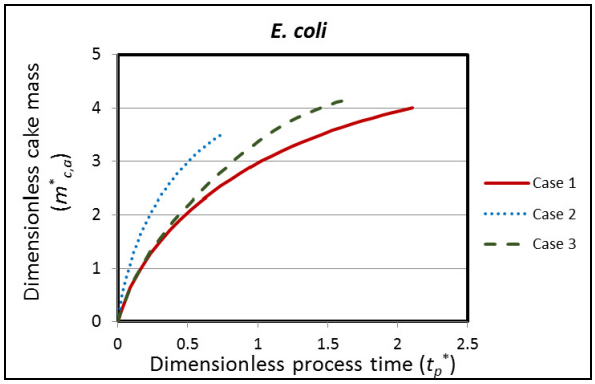

Figure 13: Predicted cake buildup with process time in the microfiltration of *E. coli* in the small-scale unit (S^* = 0.025, expt. no. 1).

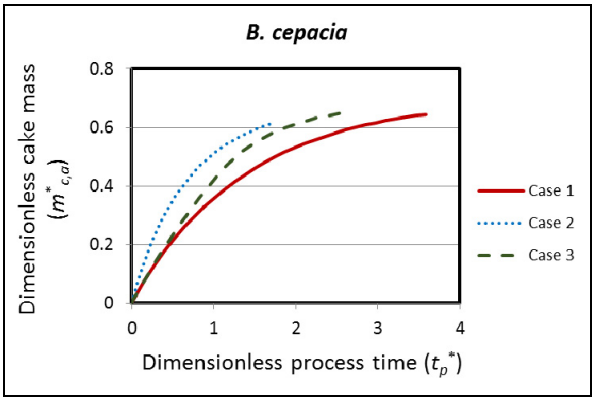

Figure 14: Predicted cake buildup with process time in the microfiltration of *B. cepacia* in the small-scale unit (S^* = 0.467, expt. no. 2).

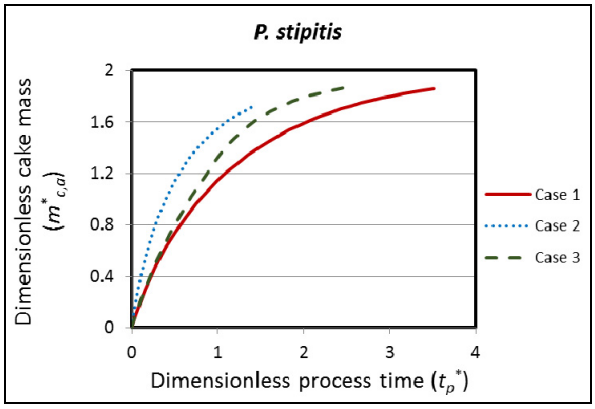

Figure 15: Predicted cake buildup with process time in the microfiltration of *P. stipitis* in the small-scale unit (S^* = 0.105, expt. no. 3).

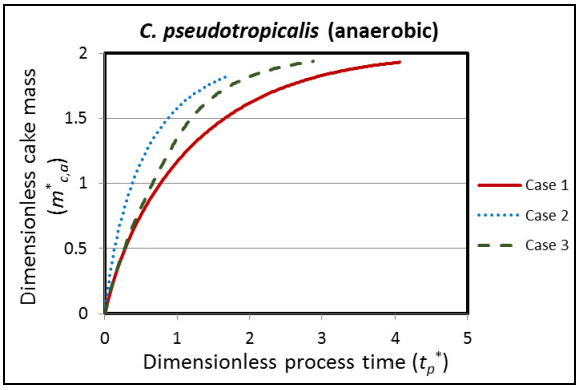

Figure 16: Predicted cake buildup with process time in the microfiltration of *C. pseudotropicalis* (grown under anaerobic conditions) in the pilot-scale unit (S^* = 0.102, expt. no. 4).

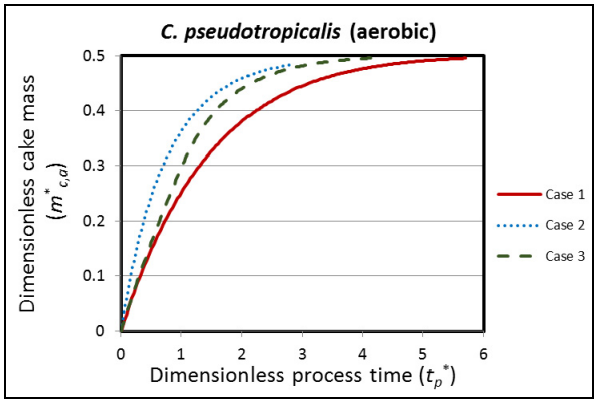

Figure 17: Predicted cake buildup with process time in the microfiltration of *C. pseudotropicalis* (grown under aerobic conditions) in the pilot-scale unit (S^* = 0.707, expt. no. 5).

If the dynamic growth of the cake mass could be experimentally measured, comparison of the theoretical values of the cake mass with the experimentally measured ones would be one way of discriminating amongst the three cases examined in this paper. It may be thought that another way to discriminate among the cases would be to estimate the surface-renewal rate S and specific cake resistance α by independent means, say from hydrodynamic and dead-end filtration measurements, and use these in the permeate-flux expressions of Table 1 to see which one of them is in closest agreement with the experimental flux. Even if such measurements were possible, as discussed earlier, it is very likely that in an actual cross-flow microfiltration run, α would depend strongly upon S, and thus its separate measurement would not be meaningful.

CONCLUSIONS

This work examined the influence of the RTD of surface elements on a model of cross-flow microfiltration that has been proposed recently (Hasan *et al*., 2013). Along with the RTD from the previous work (Case 1), two other RTD functions were used to develop theoretical equations for the permeate flux decline and cake buildup in the filter as a function of process time. The parameters of the model (R_m, k_c and S) were estimated for all three cases by fitting the appropriate expression for the permeate flux to experimental permeate-flow rate data in the microfiltration of fermentation broths in small- and pilot-scale units, which were reported in the earlier work (Hasan *et al*., 2013). The higher the values of R_m and k_c, the lower is the permeate flux. *P. stipitis* had the lowest value of k_c, followed by *B. cepacia* and *E. coli*, respectively. For the experimental runs in this work, R_m ranges from $0.090-1.922 \times 10^{13}$ m^{-1}, S ranges from $3.0-10.1 \times 10^{-4}$, $1.1-5.0 \times 10^{-4}$ and $2.3-7.6 \times 10^{-4}$ s^{-1}, while k_c ranges over $0.285–11.323 \times 10^6$, $0.141–4.152 \times 10^6$ and $0.214–8.681 \times 10^6$ s m^{-2} for Cases 1, 2 and 3, respectively. For all three cases, there is good agreement between the predicted and experimental permeate flow rates with the average RMS deviations between theoretical and experimental values being 4.6% for Cases 1 and 2, and 4.2% for Case 3, respectively. The predicted cake mass grows with process time and develops towards a steady-state value.

The three variants of the surface-renewal model examined in this work, all of which have the same three basic parameters (R_m, α and S), are based on different speculative hypotheses about the behavior of liquid elements on the membrane surface (i.e., the startup condition). From a practical point of view, they can be looked upon as different interpolation schemes for representing the curve of permeate flux as a function of process time, given the initial and long-time or steady-state values of the flux. The fact that all three variants are approximately equivalent as regards prediction of the permeate flux points to the constructive nature of the surface-renewal model – a common feature of the majority of theories or models used in science and engineering (Chatterjee, 2012).

NOMENCLATURE

A	constant in Eq. (16)	s^{-1}
c_b	mass of solids deposited in the filter per unit volume of filtrate (approximately equal to the concentration of solids in the feed or bulk liquid)	kg m^{-3}
$f(t, t_p)$	age-distribution function of liquid elements at the membrane wall	s^{-1}
$F(t, t_p)$	cumulative age-distribution function of liquid elements at the membrane wall	
$J(t)$	instantaneous permeate flux in a surface element at time t	m s^{-1}
$J_a(t_p)$	age-averaged permeate flux when the process time is t_p	m s^{-1}
$J_a^*(t_p^*)$	dimensionless age-averaged permeate flux when the dimensionless process time is t_p^*; defined by Eq. (9)	
J_{lim}	limiting or steady-state permeate flux	m s^{-1}
J_{lim}^*	dimensionless limiting or steady-state permeate flux; J_{lim}/J_0	
J_0	initial permeate flux	m s^{-1}
K	constant; assumed equal to 1	
k_c	defined by Eq. (3)	s m^{-2}
$m_c(t)$	mass of cake in a surface element per unit area of membrane surface at time t	kg m^{-2}
$m_{c,a}(t_p)$	age-averaged cake mass per unit area of membrane surface at process time t_p	kg m^{-2}
$m_{c,a}^*(t_p^*)$	dimensionless age-averaged cake mass when the dimensionless process time is t_p^*; defined by Eq. (10)	

$m^*_{c,lim}$	limiting or steady-state dimensionless cake mass	
R_m	hydraulic resistance of the membrane	m^{-1}
S	rate of renewal of liquid elements at the membrane surface	s^{-1}
S^*	dimensionless surface-renewal rate; defined by Eq. (7)	
t	residence time of a liquid element at the membrane surface	s
t^*	dimensionless residence time (= St)	
t_p	process time	s
t^*_p	dimensionless process time (= St_p)	
$u(t)$	unit step function	
x	parameter of $\Gamma(x, y)$	
y	parameter of $\Gamma(x, y)$	
z	upper limit of the integrals in Eqs. (15) and (17)	s

Greek Symbols

α	specific cake resistance	m kg^{-1}
$\Gamma(x, y)$	extended Euler gamma function; defined by Eq. (11)	
$\delta(t)$	delta function	
Δp	transmembrane pressure drop	Pa or kPa
λ	variable of integration in Eq. (11)	
μ	viscosity of the permeate	kg m^{-1} s^{-1}

REFERENCES

Almeida, A., Geraldes, V. and Semiao, V., Microflow hydrodynamics in slits: Effects of the walls relative roughness and spacer inter-filaments distance. Chem. Eng. Sci., 65, 3660-3670 (2010).

Arnot, T. C., Field, R. W. and Koltuniewicz, A. B., Cross-flow and dead-end microfiltration of oily-water emulsions. Part II: Mechanisms and modeling of flux decline. J. Membrane Sci., 169, 1-15 (2000).

Chatterjee, S. G., On the use of the surface-renewal concept to describe cross-flow ultrafiltration. Indian Chemical Engineer, 52, 179-193 (2010).

Chatterjee, S. G., The nature of scientific theory. Current Science, 102, 386-388 (2012).

Chung, B. T. F., Fan, L. T. and Hwang, C. L., Surface renewal and penetration models in the transient state. AIChE J., 17, 154-160 (1971).

Constenla, D. T. and Lozano, J. E., Predicting stationary permeate flux in the ultrafiltration of apple juice. Lebensm. Wiss. U. Technol., 29, 587-592 (1996).

Danckwerts, P. V., Significance of liquid-film coefficients in gas absorption. Ind. Eng. Chem. (Eng. and Process Dev.), 43, 1460-1467 (1951).

Fan, L. T., Shen, B. C. and Chou, S. T., The surface-renewal theory of interphase transport: A stochastic treatment. Chem. Eng. Sci., 48, 3971-3982 (1993).

Field, R. W., Wu, D., Howell, J. A. and Gupta, B. B., Critical flux concept for microfiltration fouling. J. Membrane Sci., 100, 259-272 (1995).

Gehlert, G., Luque, S. and Belfort, G., Comparison of ultra- and microfiltration in the presence and absence of secondary flow with polysaccharides, proteins, and yeast suspensions. Biotechnol. Prog., 14, 931-942 (1998).

Hasan, A., Yasarla, R., Ramarao, B. V. and Amidon, T. E., Separation of lignocellulosic hydrolyzate components using ceramic microfilters. J. Wood Chem. Technol., 31, 357-383 (2011).

Hasan, A., Peluso, C. R., Hull, T. S., Fieschko, J. and Chatterjee, S. G., A surface-renewal model of cross-flow microfiltration. Brazilian Journal of Chemical Engineering, 30, 167-186 (2013).

Ikuta, S., Personal communication (2014).

Koltuniewicz, A., Predicting permeate flux in ultrafiltration on the basis of surface renewal concept. J. Membrane Sci., 68, 107-118 (1992).

Koltuniewicz, A. and Noworyta, A., Dynamic properties of ultrafiltration systems in light of the surface renewal theory. Ind. Eng. Chem. Res., 33, 1771-1779 (1994).

Koltuniewicz, A. and Noworyta, A., Method of yield evaluation for pressure-driven membrane processes. Chem. Eng. J., 58, 175-182 (1995).

Mallubhotla, H. and Belfort, G., Flux enhancement during Dean vortex microfiltration. 8. Further diagnostics. J. Membrane Sci., 125, 75-91 (1997).

Mallubhotla, H., Hoffmann, S., Schmidt, M., Vente, J. and Belfort, G., Flux enhancement during dean vortex tubular membrane nanofiltration. 10. Design, construction, and system characterization. J. Membrane Sci., 141, 183-195 (1998).

McCabe, W. L., Smith, J. C. and Harriott, P., Unit Operations of Chemical Engineering. Fifth Ed.,

McGraw-Hill, New York (1993).

Perry, R. H., Green, D. W. and Maloney, J. O., Eds., Perry's Chemical Engineers' Handbook. Sixth Ed., McGraw-Hill, New York (1984).

Sada, E., Katoh, S., Yoshii, H. and Ban, Y., Rates of gas absorption with interfacial turbulence caused by micro-stirrers. Can. J. Chem. Eng., 57, 704-706 (1979).

Sarkar, D., Datta, D., Sen, D. and Bhattacharjee, C., Simulation of continuous stirred rotating disk-membrane module: An approach based on surface renewal theory. Chem. Eng. Sci., 66, 2554-2567 (2011).

Szwast, M., Szwast, Z., Gradkowski, M. and Piatkiewicz, W., Modelling of postproduction suspensions' concentration processes by "batch" membrane microfiltration. Chemical and Process Engineering, 34, 313-325 (2013).